https://doi.org/10.22226/2410-3535-2022-2-100-105

A study of the distribution of Au atoms in the LI_2 superstructure of the $Fe_{25}Pd_{50}Au_{25}$ alloy using field ion microscopy

V. A. Ivchenko

ivchenko2008@mail.ru

Institute of Electrophysics, UB of RAS, Yekaterinburg, 620016, Russia

The structural state of Fe-Pd-Au alloys has a significant effect on the physical properties and the character of the magnetic phase diagrams. This occurs due to changes in the competing exchange interactions between atoms. Based on the data obtained by the Mössbauer spectroscopy, two models of the distribution of gold atoms in the unit cell LI_2 as a function of the annealing temperature during ordering were proposed. The first model describes the structure of the alloy after high-temperature annealing (970 K) and assumes a statistical distribution of Au atoms over all faces of the LI_2 type unit cell. The second model describes the structure of the alloy after low-temperature annealing (720 K) and assumes that Au atoms occupy only the central nodes of the face-centered lattice in the palladium sublattice LI_2, so that the entire superstructure becomes anisotropic. Here we present the results of field ion microscopy studies on the occupancy of specific nodes in the unit cell by gold atoms in the ternary ordered alloy $Fe_{25}Pd_{50}Au_{25}$ exhibited the LI_2 superlattice. Field ion microscopy (FIM) is used to obtain data on the settlement of nodes with gold atoms in the LI_2 superstructure. It is established that Au atoms are equally likely to occupy nodes of face-centered faces in the LI_2 lattice, so that the entire superstructure becomes isotropic.

Keywords: ordered $Fe\{Pd(1-x)Au(x)\}_3$ alloys, unit cell, field ion microscopy.

1. Introduction

It was shown in [1] that the structural state of Fe-Pd-Au alloys has a significant effect on the physical properties and the character of magnetic phase diagrams. This occurs due to changes in the competing exchange interactions between atoms. Earlier [1], two models were proposed for the distribution of gold atoms distribution in the unit cell LI_2 as a function of the annealing temperature during ordering (Fig. 1b, c) were proposed, based on the data obtained by the Mössbauer spectroscopy, (Fig. 2). Figure 1a shows the arrangement of iron and palladium atoms in the unit cell of the ordered $FePd_3$ alloy.

The first model describes the structure of the alloy after high-temperature annealing (970 K) and assumes a statistical distribution of Au atoms over all faces of the LI_2 type unit cell. This distribution of Au atoms indicates that the Mossbauer spectra at 970 K have the Zeeman lines of the components arranged in perfect symmetry (Fig. 2 b). Also, this distribution of gold atoms explains the magnetic properties of the alloy, [1].

The second model, corresponding to the structure of the alloy after low-temperature annealing (720 K), assumes that Au atoms occupy only the central nodes of the face-centered lattice in the palladium sublattice LI_2, so that the entire superstructure becomes anisotropic [1]. This model explains the transition of the magnetic state of the alloy from ferromagnetic to antiferromagnetic in the process of atomic ordering at 720 K. The presence of significant quadrupole shifts of individual lines of the sextet spectra is a characteristic

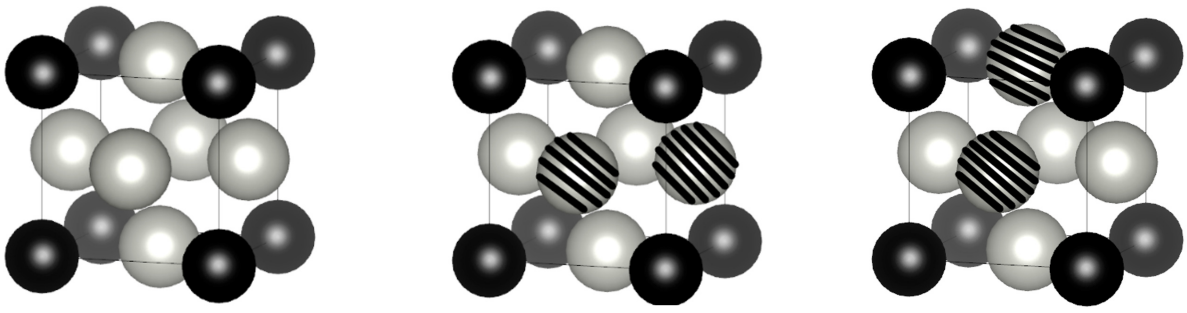

a b c

Fig. 1. The unit cell of the ordered alloy $FePd_3$ (a); possible distribution of atoms in the unit cell of $Fe_{25}Pd_{50}Au_{25}$ annealed at 720 K (b); possible distribution of atoms in the unit cell of $Fe_{25}Pd_{50}Au_{25}$ annealed at 970 K (c). Black circles — Fe atoms, grey circles — Pd atoms, dashed circles — Au atoms.

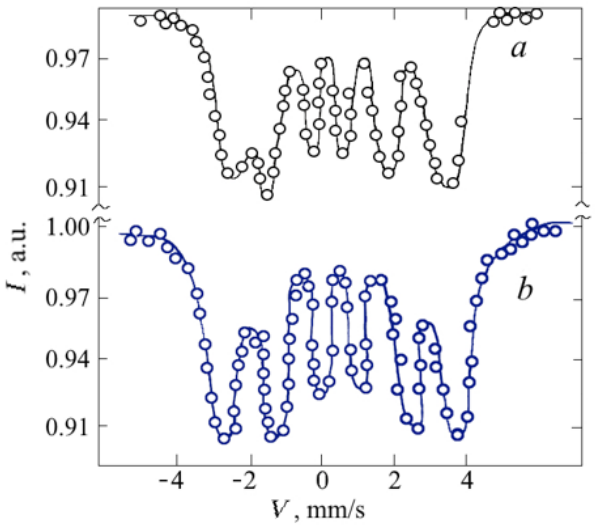

Fig. 2. Mossbauer spectra of the ordered alloy $Fe_{25}Pd_{50}Au_{25}$ annealed at 720 K during 40 h (a) and at 970 K during 1 h (b), fulfilled at 77 K [1].

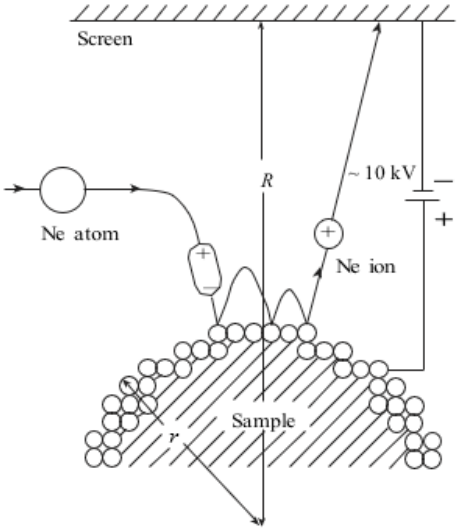

Fig. 3. Schematic representation of ion imaging of the metal surface ($r = 3 \times 10^{-6}$ cm, $R = 6$ cm, sample $T = 78$ K).

of the Mössbauer spectra for such alloys (due to the magnetic exchange interaction in Fe-Pd-Fe and Fe-Au-Fe, since the distribution at the lattice sites is different) (Fig. 2 a).

In material physics, Mössbauer spectroscopy can be used to obtain information about the geometry of the neighborhood of an atom, [2 – 5].

In transmission electron microscopy (TEM), electrons diffraction defines contrasts in an electronic image. Despite the resolution of atomic row, this method does not allow one to determine the type of an atom in atomic planes. Using field ion microscopy (FIM), one can directly study crystal lattices with atomic resolution. The latter property is the key distinction between FIM and other techniques with atomic resolutions, which are indirect methods in microscopic studies of lattices [6 – 11].

The purpose of this study is to establish the distribution of gold atoms in the unit cell of the $Fe_{25}Pd_{50}Au_{25}$ alloy ordered by type LI_2. To solve this problem, it is necessary to determine which atoms of the ordered alloy $Fe_{25}Pd_{50}Au_{25}$ give contrast in the ion image of the surface. Earlier, when studying various ordered systems in FIM, the following was established: for the Cu-Au system, contrast is given by Au atoms, [12 – 16]; for Pd-Cu by Pd atoms, [17,18]; for Pd-Cu-Ag by Pd atoms, [19, 20]; for Pt-Co by Pt atoms, [21]. The next stage of the study is the direct determination of nodes in the unit cell of the ordered alloy $Fe_{25}Pd_{50}Au_{25}$ occupied by Au atoms.

2. Experimental technique

The operating principle of a field ion microscope is based on the projective ion imaging of the sample surface and is determined by the device itself [22]. The ion image of the sample vertex surface [$r \approx (3 – 5) \times 10^{-6}$ cm] (Fig. 3) is formed on the screen by positive ions of the imaging gas (usually He, Ne) by inducing a strong electric field over the emitter surface ($\approx 5 \times 10^8$ V/cm) at a corresponding potential difference between the sample and the screen. The magnification reaches several million, and the resolution is 0.2 – 0.3 nm. The residual gas pressure in the microscope chamber can take values within $10^{-4} – 10^{-8}$ Pa, depending on the purpose.

An inert gas is used as the imaging gas, the operating pressure of which is usually $10^{-3} – 10^{-4}$ Pa and is determined by the distance between the tip and fluorescent screen, and is comparable with the mean travelling distance of the imaging gas ions. Ionization of the imaging gas occurs at a certain value of electric field and is observed at a distance no closer than the critical one from the tip end surface, ≈0.5 nm. The probability of ionization of the imaging gas above the protruding surface atoms is higher. They are arranged at plane edge atoms and are approximately estimated by the Wentzel-Kramers-Brillouin (WKB) relation [22]. Such an event becomes probable due to the tunneling effect.

Therefore, the image observed on the microscopic screen in Fig. 4, on the one hand, represents the contrast of the tip end surface from atoms at the step edges, on the other, reflects the stereographic projection of the crystal under study. The

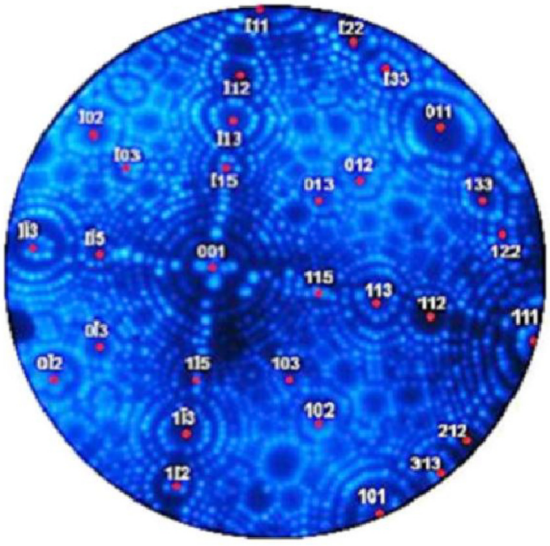

Fig. 4. (Color online) Neon image of Pt single crystal, $U = 10$ kV.

circular contour lines on the ion image represent the edges of the corresponding families of crystallographic planes of certain directions. Adjacent rings (from any family of concentric rings) represent images of parallel atomic layers. The distance between rings corresponds to the interplane distance for a given crystallographic direction. In terms of ion microscopic picture, this distance is also referred to as the lattice step height. The rings themselves in the ion microscopic picture, as a rule, consist of separate bright dots, which are images of surface atoms arranged at atomic sites at the step edges.

Imaging of the ion microscopic picture of the sample surface by the radial projection is directly associated with the possibility of preparing the emitter tip shaped as an almost hemispherical atomically smooth surface. This is achieved by using field evaporation, which occurs only at sufficiently high value of electric field over the emitter surface. This field induces the protruding surface atoms to "evaporate" in the form of positive ions. Field evaporation is a self-controlled process of "polishing" tip apex, since the local electric field enhancement near sharp edges and over bumps results in their preferential "evaporation" (removal) by the field. As a result, the tip apex surface becomes ideally smooth on an atomic scale. Furthermore, this permanently visualized during field evaporation surface is atomically clean. Continuous recording of such a surface using photo, video, or movie cameras during controlled layer by layer removal of surface atoms makes it possible to analyze the crystal structure of the object of study in the material volume.

The samples for the study in FIM were prepared in the form of needle emitters with a curvature at the vertex of 30 – 50 nm by electrochemical polishing. The blanks consisted of pre-ordered alloys of $Fe\{Pd(1-x)Au(x)\}_3$. To obtain an ordered alloy, $Fe_{25}Pd_{50}Au_{25}$ was subjected to heat-treatment: (1) one hour annealing at $T = 970$ K and (2) 40 hours annealing at $T = 720$ K.

During the study, the tips of the field emitters had an atomically smooth surface, close to hemispherical. Such an atomically pure surface is obtained in situ by field evaporation of the surface atoms. This was necessary for further study of the atomic structure of the research. Then, field ion images of the surface with controlled removal of atomic layers were recorded, using the recording equipment (photo or video camera), and the structural state of the alloy in the volume was analyzed. The field ion microscope was equipped with a microchannel ion-electron converter that enhances the brightness of ion images by 10^4. Liquid nitrogen ($T = 78$ K) served as the refrigerant, and spectrally pure neon was used as the imaging gas.

3. Results and discussion

Analysis of the field ion images of superstructural layers of the binary $FePd_3$ alloy showed that only rings of mixed Fe-Pd planes are depicted (Fig. 5).

Hence, it is obvious that Pd atoms are not depicted on the screen of a field ion microscope [14,18,19], and Fe atoms give contrast in the form of bright image points on the micro-maps of the surface. This fact is proved by the presence of contrasting antiphase boundaries (AFG) crossing the faces of the superstructural poles (001) and (011) (Fig. 5).

According to the results of Mössbauer studies after annealing (970 K), the distribution of gold atoms in the superstructure of the $FePd_2Au$ alloy is statistical, Fig. 1c [1]. Gold atoms statistically occupy the central nodes of the face-centered lattice, thus, an appearance of ion contrast of Pd-Au atomic layers, which in $FePd_3$ alloy did not give any contrast, with an increase of gold concentration indicates that gold atoms are depicted on the screen of a field ion microscope (FIM) (Fig. 6). With an increase in the concentration of Au atoms in $Fe\{Pd(1-x)Au(x)\}_3$ alloys, the contrast of the Pd-Au atomic layers becomes almost identical in brightness with the contrast of the Fe-Pd atomic layers (Fig. 6).

Thus, the results of FIM studies of ordered alloys of the $Fe\{Pd(1-x)Au(x)\}_3$ system (gold content: 5, 12.5, 20 and 37.5 at.%) show that Pd atoms do not produce images in the form of contrasting points (hereinafter referred to as atoms) on the FIM screen. Fe atoms give the main contrast, while Au atoms give the identical contrast in brightness relative to the contrast of Fe atoms, Fig. 6.

For both models, almost the same contrast of rings from alternating planes filled with gold and palladium atoms in the ordered $Fe_{25}Pd_{50}Au_{25}$ alloy is observed. As a rule, the contrast from ordered binary alloys in FIM is created by atoms of the same type. Therefore, there is a contrast of the

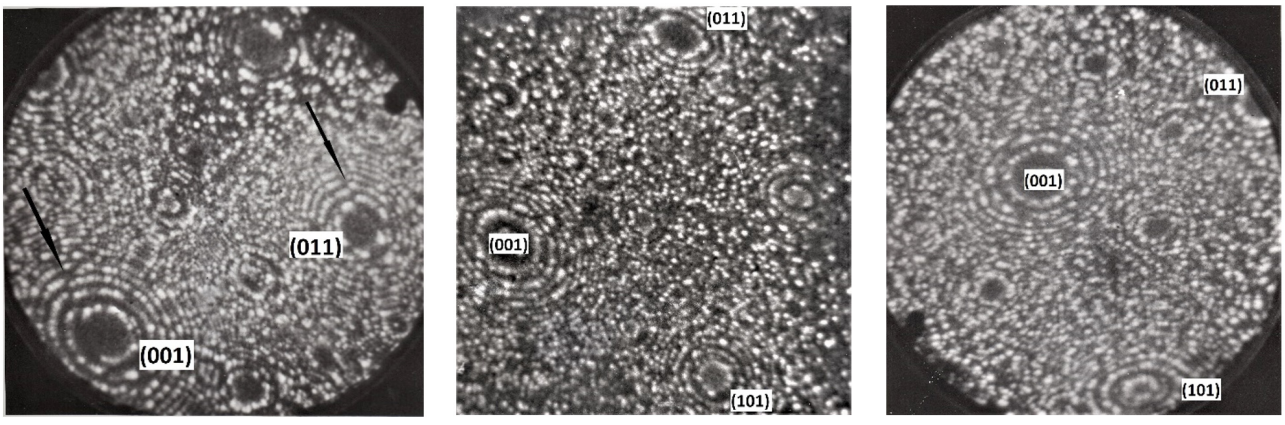

a b c

Fig. 5. Field ion image of the surface of $FePd_3$ alloy, having LI_2 type ordering, black arrows indicate the antiphase boundaries (a); field ion image of the surface of $Fe_{25}Pd_{50}Au_{25}$ alloy, having structure following low-temperature annealing (720 K) (b); field ion image of the surface of $Fe_{25}Pd_{50}Au_{25}$ alloy, having structure following high-temperature annealing (970 K) (c).

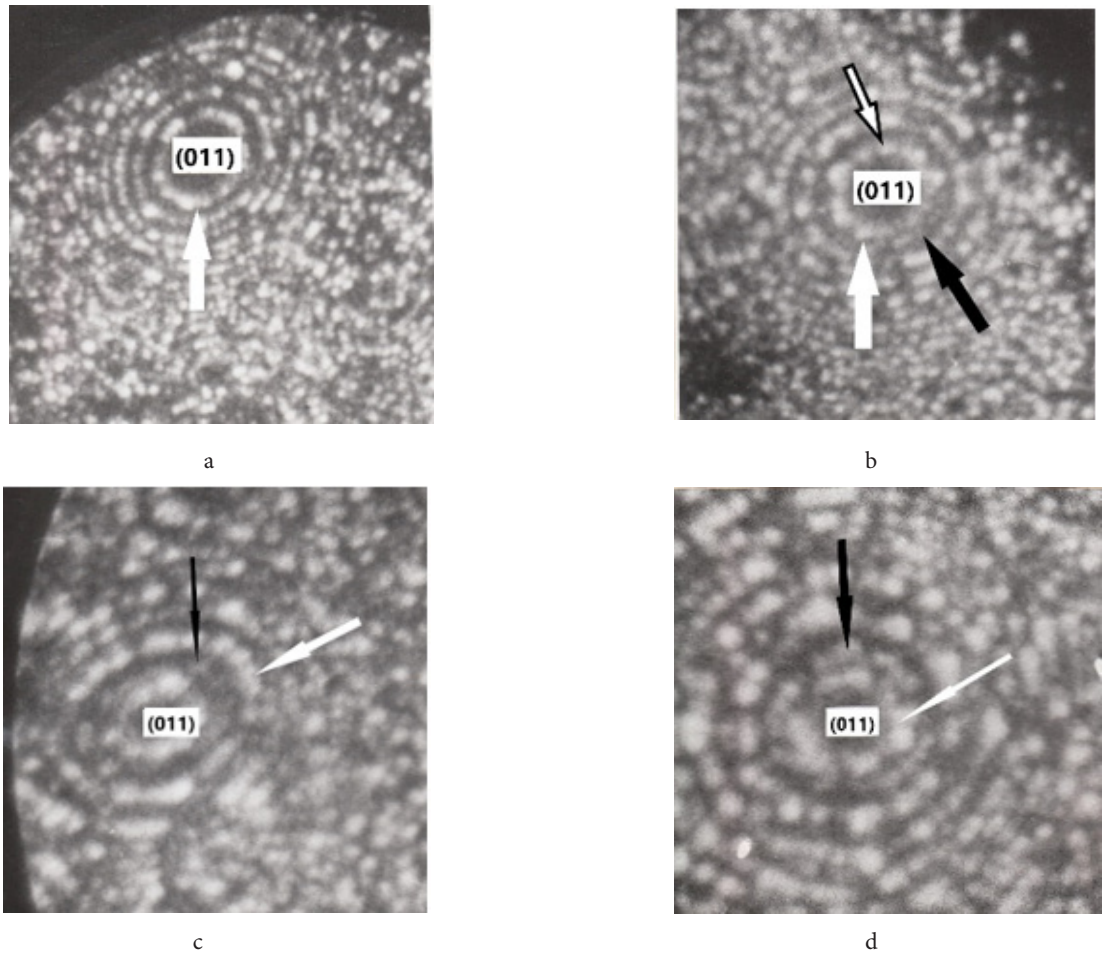

Fig. 6. FIM images of the surface of $Fe\{Pd(1-x)Au(x)\}_3$ alloys system depending on the Au content in the region of (001) pole. $x=5\%$ (a), $x=12.5\%$ (b), $x=20\%$ (c), $x=37.5\%$ (d). White arrows indicate rings of Fe-Pd atomic layers. The black arrows indicate the rings of Pd-Au atomic layers. The black and white arrow indicates the image of a single atom.

so-called "double" step [12]. At the same time, only the rings, filled with atoms create contrast and are depicted on the FIM screen. In the case of the ordered $FePd_3$ alloy, the image is created only by Fe atoms. Therefore, the rings are observed only from the Fe-Pd planes and, accordingly, there is a the "double" step contrast of, and the composition of these mixed planes is 50% Fe and 50% Pd.

If we assume that the first model is satisfied (annealing 970 K), then the contrast rings from the (Fe, Pd, Au) planes of the $Fe_{25}Pd_{50}Au_{25}$ alloy will differ from the rings (Fe, Pd) in the similar planes of the $FePd_3$ alloy, since gold atoms should be statistically present in the $Fe_{25}Pd_{50}Au_{25}$ unit cell (see Fig. 5).

It remains to establish the distribution of gold atoms over the superlattice faces. It is obvious from the experimental data that with an increase in the number of gold atoms (37.5%) in the $Fe\{Pd(1-x)Au(x)\}_3$ alloy, the number of image points of atoms in the rings of the palladium sublattice increases (Fig. 6). This is possible only if gold atoms are depicted in "palladium" planes. It follows that gold atoms replace palladium atoms in the "palladium" planes. A comparison of the ion images of the $Fe\{Pd(1-x)Au(x)\}_3$ alloys with the micro-image of the $FePd_3$ alloy makes it possible to determine that the number of image points of atoms in the "palladium" planes increases with an increase in the concentration of gold atoms in the alloy, and the brightness of the image of gold atoms is comparable to the brightness of the image of Fe atoms. In the $FePd_3$ alloy, the resolution of the image points of Fe atoms is clearly observed in the rings of the depicted mixed planes, since Pd atoms are located between Fe atoms, but do not give images. In comparison with the same rings of alloys with a concentration of gold (37.5%), there is almost complete filling with dots in the image by atoms in the rings of mixed planes containing Pd, Au atoms, see Fig. 6 d.

Let us proceed to the analysis of the contrast of superstructural faces of type {001} in ordered $Fe_{25}Pd_{50}Au_{25}$ alloys at 970 and 720 K. Figure 7 shows the contrast from the faces of type {001} at the corresponding temperatures. There is almost no difference in contrast from the planes of the palladium sublattice. Annealing of the alloy at 970 K shows a contrast with the filling of the image points of gold atoms in the Pd sublattice (Fig. 7a). The contrast after annealing of the alloy at 720 K is identical and shows almost the same density of filling with Au atoms. The contrast points of Au atoms in the "palladium" planes of the alloy (720 K) are about 25%.

According to our estimate, the contrasts in Fig. 7a and 7b are identical. Therefore, it can be concluded with confidence that Au atoms are equally likely to occupy the central nodes of the face-centered lattice in the LI_2 superlattice, so that the entire superstructure of the $Fe_{25}Pd_{50}Au_{25}$ alloy becomes isotropic.

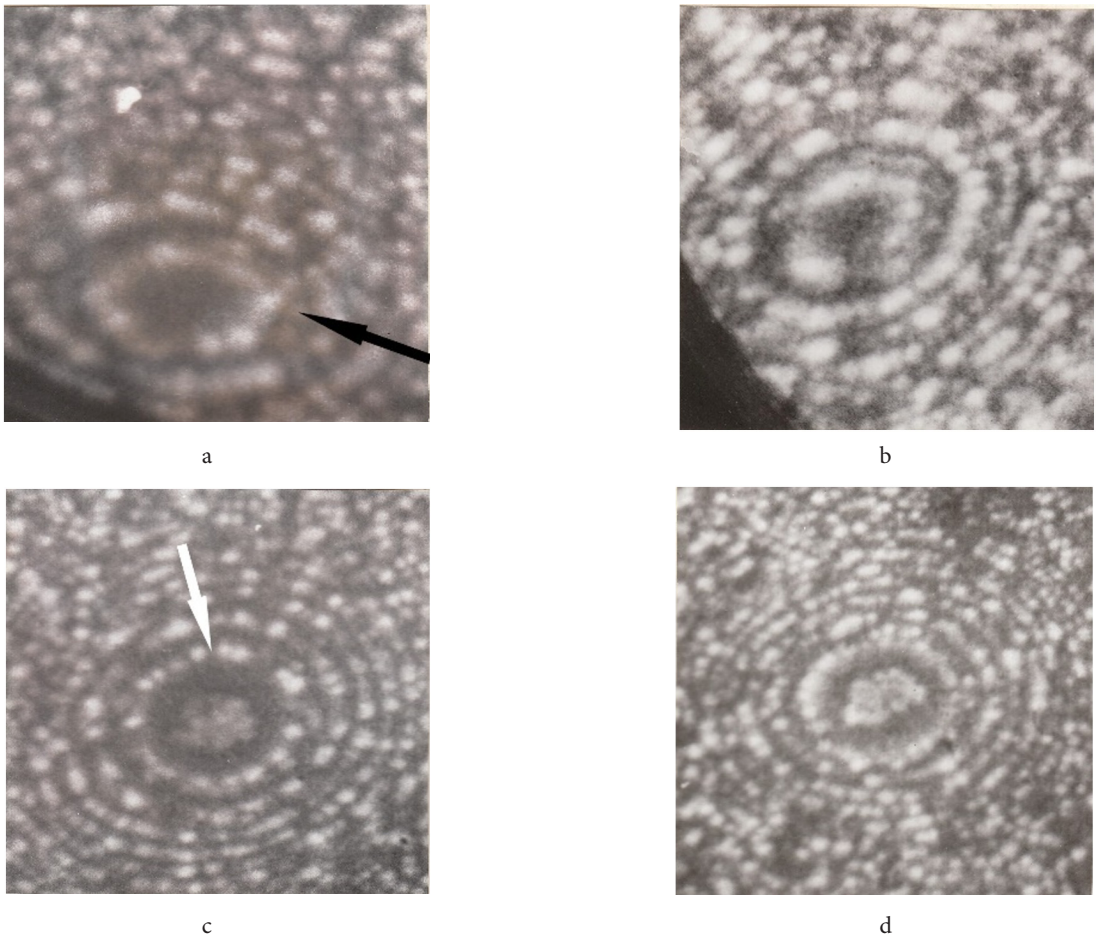

Fig. 7. Field ion images of the surface of $Fe_{25}Pd_{50}Au_{25}$ alloy in the region of (011) pole: $T = 970$ K (a), the black arrow indicates the rings of Pd-Au atomic layers; $T = 720$ K (b). Field ion images of the surface of $Fe_{25}Pd_{50}Au_{25}$ alloy in the region of (001) pole: $T = 970$ K (c); $T = 720$ K (d). The white arrow indicates the image of the atom in the form of a vacancy.

The first model is confirmed by the contrast from superstructural faces of type {011} (Fig. 7c, d). For the first model (970 K), there is a contrast from alternating planes, where Au and Pd atoms are equally likely to be located (see Fig. 7b). It is necessary to notice the presence of Pd atoms in these rings (Pd atoms do not give contrast), but are observed in the form of "vacancies" in the rings. Therefore, images of Au atoms in rings are depicted as individual atoms. In accordance with the second model, the contrast from the faces of type {011} is formed by alternating layers, Fig. 1b. In the faces containing only Fe and Pd atoms, the identical contrast of the same faces in the $FePd_3$ alloy is observed (Fig. 7c, d). But in the $Fe_{25}Pd_{50}Au_{25}$ alloy, the atomic faces (Pd, Au) alternating with the faces (Fe, Pd) have a contrast due to the presence of Au atoms in them. Only when there is 50% Au in the composition of the atomic layers, the contrast from the (Pd, Au) planes will be identical to the contrast of the (Fe, Pd) planes. Figure 7 shows that the contrast of (Pd, Au) planes is not identical to the contrast of (Fe, Pd) planes. It should be emphasized that there is no double step contrast in superstructural faces because both Fe-Pd-Au atomic planes and Pd-Au atomic planes are depicted. The experimental data suggests that the first model of the distribution of atoms in the superstructure of the $Fe_{25}Pd_{50}Au_{25}$ alloy is correct.

4. Conclusions

A field ion microscopy study of the $Fe_{25}Pd_{50}Au_{25}$ alloy annealed at $T = 970$ K showed that Au atoms are equally likely occupied the central nodes of the face-centered lattice in the alloy lattice which exhibits the LI_2 unit cell (a schematic representation of the unit cell is shown in Fig. 1c). This distribution of Au atoms leads to the formation of an isotropic LI_2 superstructure in the $Fe_{25}Pd_{50}Au_{25}$ alloy.

Acknowledgements. I express my gratitude to V. V. Ivchenko for the help in editing the article.

References

1. B. V. Ryzhenko, F. A. Sidorenko, P. V. Geld. B. V. Phys. Solid State. 33 (3), 741 (1991). (in Russian)
2. B. V. Ryzhenko, S. V. Pridvizhkin, P. V. Geld. Hyperfine Interactions. 72 (4), 313 (1992). Crossref
3. B. V. Ryzhenko, S. V. Pridvizhkin, P. V. Geld. Journal of Magnetism and Magnetic Materials. 89 (1-2), 236 (1990). Crossref
4. S. V. Pridvizhkin, B. V. Ryzhenko, P. V. Geld. Soviet Physics Journal. 32 (8), 617 (1990).

5. B. V. Ryzhenko, B. Yu. Goloborodkyi, F. A. Sidorenko. Phys. Solid State. 26 (6), 1795 (1984). (in Russian)
6. D. G. Brandon. J Sci Instrum. 41, 373 (1964).
7. A. Cerezo, M. Hetherington, J. Hyde, M. Miller, G. Smith. Surf Sci. 280, 471 (1992).
8. F. Danoix, T. Epicier, F. Vurpillot, D. Blavette. J Mater Sci 47 (3), 1567 (2012). Crossref
9. M. Dagan, L. R. Hanna, A. Xu, S. G. Roberts, G. D. Smith et al. Ultramicroscopy. 159, 387 (2015).
10. R. Xu, C. C. Chen, L. Wu, M. C. Scott et al. Nat Mater. 14, 1099 (2015).
11. F. Vurpillot, M. Gilbert, B. Deconihout. Surf Interface Anal. 39, 273 (2007).
12. V. A. Ivchenko, N. N. Syutkin. The Physics of Metals and Metallography. 61 (3), 575 (1986). (in Russian)
13. V. A. Ivchenko, N. N. Syutkin, A. Kvist, H.-O. Andrén, K. Stiller. Applied Surface Science. 94 – 95, 267 (1996). Crossref
14. A. U. Bunkin, V. A. Ivchenko, L. U. Kuznetsova, N. N. Syutkin. The Physics of Metals and Metallography. 7, 111 (1990). (in Russian)
15. V. A. Ivchenko, N. N. Syutkin, Y. F. Talantsev. The Physics of Metals and Metallography. 69 (2), 118 (1990).
16. V. A. Ivchenko. Surface Science. 276 (1-3), 273 (1992).
17. N. N. Syutkin, V. A. Ivchenko, S. I. Noritsin, A. B. Telegin. Fizika metallov i metallovedeniye. 56 (4), 728 (1983). (in Russian)
18. V. A. Ivchenko, E. V. Popova, T. S. Gorskikb. The Physics of Metals and Metallography. 97 (2), 207 (2004).
19. N. N. Syutkin, V. A. Ivchenko, S. I. Noritsin. The Physics of Metals and Metallography. 57 (4), 776 (1984). (in Russian)
20. N. N. Syutkin, V. A. Ivchenko, S. I. Noritsyn. Phys. Solid State. 25 (10), 3055 (1983). (in Russian)
21. V. A. Ivchenko, E. I. Teytel, N. N. Syutkin. The Physics of Metals and Metallography. 52 (1), 164 (1981). (in Russian)
22. E. V. Myuller. Field Ionization and Field Ion Microscopy. Phys. Usp. 77, 481 (1962).